Article

UDC 621.793

https://doi.org/10.31489/2026PH1/22-39

Received: 06.10.2025
Accepted: 18.12.2025

A.B. Kengesbekov[1, 3, 4], A.Zh. Zhassulan[1, 2], N. Muktanova[1, 3], Daryn Baizhan[1, 2], E. Akhmetova[1, 3], A. Serikbaikyzy[1]✉

[1]*D. Serikbayev East Kazakhstan Technical University, Ust-Kamenogorsk, Kazakhstan;*
[2]*Engineering Center, Shakarim University NJSC, Semey, Kazakhstan;*
[3]*PlasmaScience LLP, Ust-Kamenogorsk, Kazakhstan;*
[4]*Institute of Composite Materials, Ust-Kamenogorsk, Kazakhstan*

Incorporating TiO_2 Nanoparticles to Enhance Corrosion Resistance, Cytocompatibility of PEO Calcium–Phosphate Coatings on Titanium

Titanium and its alloys are widely used in biomedical implants due to their favorable mechanical properties and corrosion resistance; however, their natural surface lacks sufficient bioactivity. Micro-arc oxidation is a promising approach to producing bioactive coatings, and the incorporation of nanoparticles such as TiO_2 may further improve their functionality. This study aimed to determine the optimal TiO_2 nanoparticle concentration in the micro-arc oxidation electrolyte that ensures coating stability and biological safety. Calcium–phosphate coatings were fabricated on commercially pure titanium using micro-arc oxidation with two TiO_2 concentrations: 0.5 wt.% (MAO 1) and 1 wt.% (MAO 2). Surface morphology, porosity, and phase composition were analyzed by scanning electron microscopy, energy-dispersive spectroscopy, and X-ray diffraction. Corrosion resistance was evaluated via potentiodynamic polarization in NaCl and Ringer's solutions, while biocompatibility was assessed in vitro using HOS human osteosarcoma cells and MTT assays. Increasing the TiO_2 content to 1 % decreased coating porosity (13.7 % vs. 26.3 % for MAO 1), enhanced corrosion protection, and reduced the friction coefficient compared to bare titanium. However, MAO 2 exhibited high cytotoxicity (81 % cell death) and partial structural degradation in the biological medium. MAO 1 maintained integrity and showed no toxic effects (3 % cell death). These results suggest that 0.5 % TiO_2 is the optimal concentration, providing a balance between corrosion resistance, mechanical stability, and biocompatibility, supporting the development of safer implant coatings.

Keywords: micro-arc oxidation; titanium; TiO_2 nanoparticles; corrosion; biocompatibility; cytotoxicity

✉*Corresponding author*: Serikbaikyzy, Ainur, ainura.serikbaikyzy@gmail.com

Introduction

Titanium and its alloys are among the most widely used materials in modern medicine due to their high corrosion resistance, low density, favorable mechanical properties, and good bioinertness under physiological conditions [1, 2]. However, the natural surface of titanium has several limitations, such as low wear resistance and limited osseointegration [3, 4]. These factors drive the search for effective surface modification methods capable of improving the functional characteristics of titanium implants [5].

Various technologies are employed for the surface modification of titanium implants, including anodic oxidation, plasma spraying, sol-gel methods, laser texturing, ion implantation, and others [6–9]. These ap-

proaches allow the formation of oxide or bioactive layers that enhance cell adhesion and improve the corrosion resistance of the material. However, they also have several limitations, including poor coating adhesion to the substrate, insufficient porosity that slows down the osseointegration process, and challenges in the controlled incorporation of functional elements into the layer composition [10, 11]. Micro-arc oxidation (MAO) is one of the most promising methods for producing bioactive coatings on titanium [12, 13]. During MAO, a multilayered oxide film with a well-developed porous structure forms on the surface, increasing the contact area with biological tissues and enhancing osseointegration [14]. The additional incorporation of nanoparticles of various elements (Ag, Zn, Cu, TiO_2, CeO_2, etc.) into the coating can impart antibacterial, osteogenic, and photocatalytic properties [15–17], making MAO a versatile tool for the development of medical implants.

Particular attention has been given to TiO_2 nanoparticles, which are widely used due to their bioinertness, photocatalytic activity, and ability to enhance the corrosion and mechanical resistance of coatings [18–20]. However, growing evidence indicates potential toxicological risks associated with the migration of TiO_2 nanoparticles from coatings into biological environments. In vivo and in vitro studies have demonstrated that nanoparticles can penetrate tissues and organs, accumulate in the liver, kidneys, and brain, and cause oxidative stress, cell membrane damage, and apoptosis [21–24]. These effects depend on the concentration, size, and degree of nanoparticle aggregation, as well as the stability of the coating in physiological media.

Recent review and experimental studies have confirmed the promising potential of MAO coatings while highlighting the need for precise control over the composition and dosage of incorporated ions. For instance, electrochemical modification of titanium with Zn, Cu, Ag, Sr, and Ce ions via MAO has been shown to enhance osteogenic, angiogenic, and antibacterial properties. However, systematic reviews emphasize the risk of uncontrolled ion release and coating instability during long-term exposure to physiological environments [25–29].

In vitro studies on cell cultures further underline the dose-dependent nature of TiO_2 toxicity: high nanoparticle concentrations can induce oxidative stress, DNA damage, and cell cycle disruptions, particularly in three-dimensional models that mimic in vivo conditions. This highlights the increased cellular sensitivity to nanoparticle dosage and morphology and underscores the need for a comprehensive analysis of both the physicochemical and biological properties of such coatings [30, 31].

Despite the widespread use of TiO_2-modified coatings in implantology, the mechanisms underlying their potential cytotoxicity at different nanoparticle concentrations remain unclear. A comprehensive study, combining physicochemical characterization and biological testing, is required to assess coating stability and safety for living cells.

The aim of this work is to provide a systematic evaluation of the influence of TiO_2 nanoparticle concentration in the MAO electrolyte on the morphology, phase composition, corrosion resistance, and cytotoxicity of calcium–phosphate coatings formed on titanium. The findings of this study are expected to help define optimal MAO processing conditions that ensure a balance between mechanical and corrosion stability and biological safety, which is essential for the development of next-generation implantable medical devices.

Materials and methods of experiments

Commercially pure titanium (grade VT1-0) samples with dimensions of 10×10×3 mm were used in this study. Prior to treatment, the sample surfaces were subjected to mechanical grinding, ultrasonic cleaning in ethanol, rinsing with deionized water, and sandblasting to remove the native oxide layer and level the surface. Calcium–phosphate coatings were produced by micro-arc oxidation (MAO) in an aqueous electrolyte containing 30 % phosphoric acid (H_3PO_4), 60 g L^{-1} hydroxyapatite (HA), and 90 g L^{-1} calcium carbonate ($CaCO_3$). To investigate the effect of TiO_2 nanoparticle concentration, two electrolyte compositions were prepared, containing 0.5 % and 1 % TiO_2 nanoparticles, respectively. Samples obtained under these conditions are hereafter designated as MAO 1 (0.5 % TiO_2) and MAO 2 (1 % TiO_2). In addition to the TiO_2-containing coatings, a control PEO coating was prepared in the same calcium–phosphate electrolyte without TiO_2 nanoparticles (denoted MAO 0) to provide a reference for comparison of the morphological and physicochemical properties. We used commercial titanium (IV) oxide nanopowder (anatase phase) purchased from Aldrich (catalogue No. 637254-50G, Lot No. MKCN0838). According to the manufacturer's specifications, the particles have an average size of <25 nm, a purity of 99.7 %, and the crystalline phase is anatase. The base electrolyte for micro-arc oxidation was a calcium–phosphate solution consisting of 30 % H_3PO_4, 60 g L^{-1} hydroxyapatite, and 90 g L^{-1} $CaCO_3$. For the MAO 1 and MAO 2 samples, this same calcium–

phosphate electrolyte was used, with the only difference being the addition of 0.5 wt.% or 1 wt.% of the TiO_2 nanopowder described above. The MAO process was performed using a KP-HI-F-40A600V pulsed power supply under the following parameters: voltage — 300 V, processing time — 600 s, frequency — 200 Hz, duty cycle — 15 %, and current density — 0.23–0.35 A/cm^2. After treatment, the samples were rinsed with deionized water and dried at room temperature.

The surface morphology and elemental composition of the coatings were analyzed using a Tescan scanning electron microscope equipped with an energy-dispersive spectroscopy (EDS) detector. Phase composition was determined by X-ray diffraction (X'Pert PRO, PANalytical, Almelo, The Netherlands). Porosity and average pore size were quantified based on SEM images using the ImageJ software.

Corrosion resistance was evaluated by potentiodynamic polarization using a CS350M potentiostat-galvanostat (Corrtest Instruments) with a flat-type corrosion cell (model CS936) in a standard three-electrode configuration. The working electrode was a coated or uncoated sample with an exposed area of 1 cm^2. A saturated Ag/AgCl electrode served as the reference, and a platinum mesh was used as the counter electrode. Tests were conducted in two media: 3.5 wt.% NaCl and Ringer's solution at 25 °C. Prior to polarization, the open-circuit potential (OCP) was stabilized for 30 min. The potential sweep was carried out from −0.25 V to 0.00 V versus Ag/AgCl at a scan rate of 0.5 mV/s. The open surface porosity and pore size were quantified from plan-view SEM micrographs in ImageJ. After scale calibration images were segmented (Otsu threshold) with watershed separation; edge-touching features and objects < 2 μm were excluded. For each condition, 5 random fields of view were analyzed; the results are reported as mean ± SD. Static water contact angles were measured using a goniometer SDA-100 contact goniometer (Qchaida, Dongguan, China, sessile-drop method (3 μL), at 23 ± 1 °C.

Tribological tests were performed using an Anton Paar TRB3 tribometer in a ball-on-disk configuration in Ringer's solution. As the counterbody, we used a 6 mm silicon–nitride (Si_3N_4) ceramic ball, supplied with the instrument, with an applied load of 2 N and a sliding distance of 100 m. The friction coefficient was recorded in real time. Si_3N_4 was chosen because it is chemically inert and does not corrode in Ringer's solution, allowing the tribological response of the coating itself to be evaluated without interference from the counterbody.

For cytotoxicity evaluation, 10 samples were prepared (5 from each coating group). The study was carried out using the HOS human osteosarcoma cell line in accordance with ISO 10993-5 [32]. The cell concentration was 10^5 cells/mL in culture medium (90 % DMEM, 10 % FBS, antibiotics, and L-glutamine). Samples were incubated with the cell culture for 24 h at 37 °C, 5 % CO_2, and 100 % humidity. A culture without samples served as the control. After incubation, samples were removed, and 0.5 % MTT solution (NeoFroxx, Germany) was added and incubated for an additional 4 h, followed by dissolution of the formazan crystals in 10 % dodecyl sulfate in 0.01 M HCl. Optical density was measured using a Multiskan FC spectrophotometer (Thermo Fisher Scientific, China) at 540 nm with a 630 nm reference. The cytotoxicity index (CI, %) was calculated using the following formula:

$$CI\ (\%) = (K - O) / K \times 100\ \% \quad (1)$$

where K is the absorbance of the control and O is the absorbance of the sample. Samples were considered non-cytotoxic when CI ≤ 30 %. Macro- and microscopic images of the surfaces before and after the experiments were taken using a Canon Power Shot A630 digital camera and an ADF I350 inverted metallographic microscope after staining fixed cells with a mixture of Azure II and eosin. Statistical analysis was performed in RStudio (R) using the Shapiro-Wilk test (with Royston's correction), Welch's ANOVA, the Brunner-Munzel test, and Games-Howell multiple comparisons, with a significance level of $p < 0.05$. Prior to cell contact, specimens were rinsed 3× with deionized water (and PBS), then air-dried; after MAO, all samples were rinsed and dried as described.

Results of the research

Surface Morphology of MAO Coatings

Figure 1 presents the surface morphology of the coatings produced in electrolytes with different TiO_2 nanoparticle contents. The MAO 0 surface, obtained without nanoparticle addition, exhibits the typical micro-arc oxidation (MAO) morphology: a porous layer with rounded discharge craters of various sizes and relatively smooth, dense pore walls. When 0.5 wt.% TiO_2 nanoparticles are introduced into the electrolyte (MAO 1, Figure 1*b*), the coating retains the characteristic MAO structure but shows a slightly denser arrangement of pores and more uniform pore distribution. Increasing the nanoparticle concentration to 1 wt.%

produces a surface with reduced total open porosity and partial closure of some discharge channels; the large craters remain but their number is lower, indicating a more compact oxide layer. XRD analysis confirms the presence of TiO_2 signals in both MAO 1 and MAO 2 coatings, demonstrating that the TiO_2 nanoparticles become incorporated into the MAO layer during plasma-electrolytic oxidation. The amount of incorporated TiO_2 increases with the nanoparticle content in the electrolyte, but no qualitative difference in the type of incorporated phase is observed. Thus, the main effect of increasing TiO_2 concentration is a denser, less porous microstructure with a higher level of TiO_2 incorporation, which can influence the subsequent corrosion resistance and biological response.

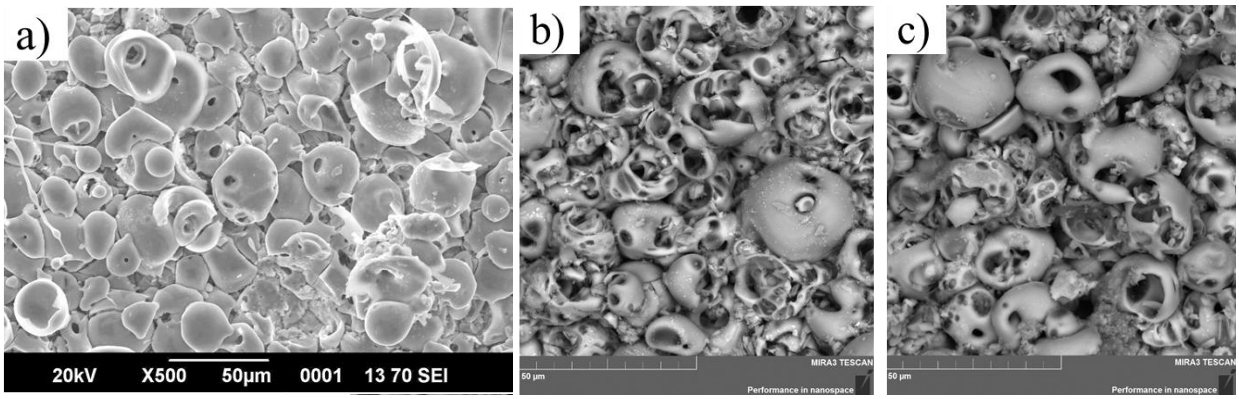

(*a*) MAO 0 — coating formed in the calcium–phosphate electrolyte without TiO_2 nanoparticles, (*b*) MAO 1 — coating formed with 0.5 wt.% TiO_2, (*c*) MAO 2 — coating formed with 1 wt.% TiO_2

Figure 1. Surface SEM images of the coatings

Phase Composition

Figure 2 presents the X-ray diffraction (XRD) patterns of the untreated titanium surface and the MAO coatings produced with different TiO_2 nanoparticle concentrations.

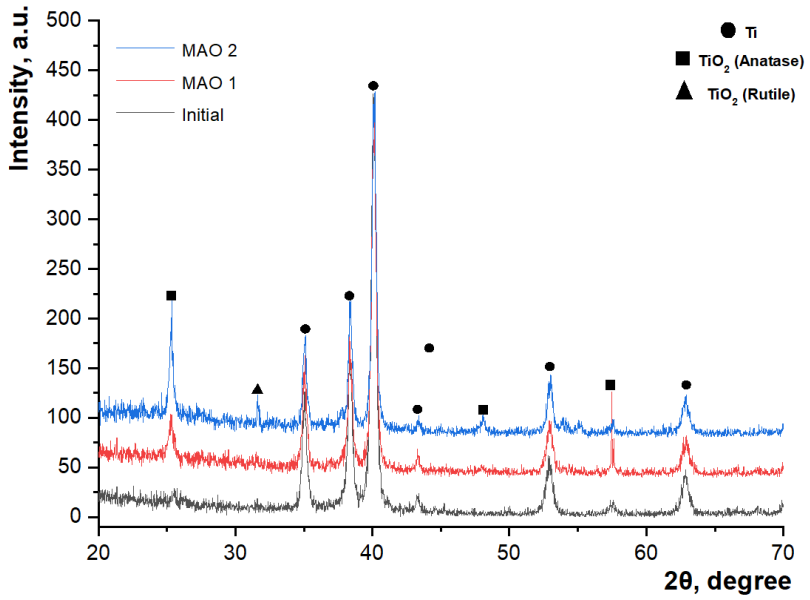

Figure 2. X-ray diffraction patterns of initial titanium and coatings containing TiO_2

For the uncoated titanium substrate, characteristic diffraction peaks of α-Ti are observed at 2θ ≈ 35°, 38°, 40°, 53°, and 63°, corresponding to the hexagonal close-packed crystal structure of metallic titanium. After MAO treatment, additional diffraction peaks appear for both coating types (MAO 1 and MAO 2), which can be attributed to titanium dioxide phases. Distinct peaks of anatase TiO_2 are detected at approximately 2θ ≈ 25°, 37°, 48°, and 55°, while rutile peaks are observed to a lesser extent near 2θ ≈ 27°. This in-

dicates the formation of an oxide film with a mixed polymorphic composition. Increasing the TiO_2 nanoparticle concentration in the electrolyte (MAO 2) results in a higher intensity of both anatase and rutile peaks compared to MAO 1, suggesting a greater amount of crystalline TiO_2 phases in the coating [33, 34]. The metallic titanium peaks remain visible, which is attributed to partial penetration of the X-ray beam through the porous coating layer to the underlying substrate. Thus, a higher TiO_2 nanoparticle content promotes the formation of a coating with enhanced crystallinity and enrichment in the anatase and rutile phases.

Porosity and Pore Size

In aqueous electrolytes, such particles can form loose agglomerates of several hundred nanometers, which is typical for unmodified TiO_2 suspensions in near-neutral or weakly alkaline solutions [35]. During micro-arc oxidation, the local plasma micro-discharges reach transient temperatures of 2000–10,000 K, but the residence time of individual nanoparticles in the discharge channel is extremely short (micro- to milliseconds) and rapid quenching occurs [36]. Numerous studies have shown that TiO_2 nanoparticles do not melt completely; instead, they become partially sintered and are incorporated into the growing calcium–phosphate/TiO_2 oxide layer as crystalline anatase/rutile phases [37]. Our own XRD and EDS analyses (Figures 2 and 12) confirm the presence of anatase and rutile peaks in the final coating, demonstrating that TiO_2 nanoparticles survive the MAO process and are embedded within the oxide matrix rather than being dissolved or lost.

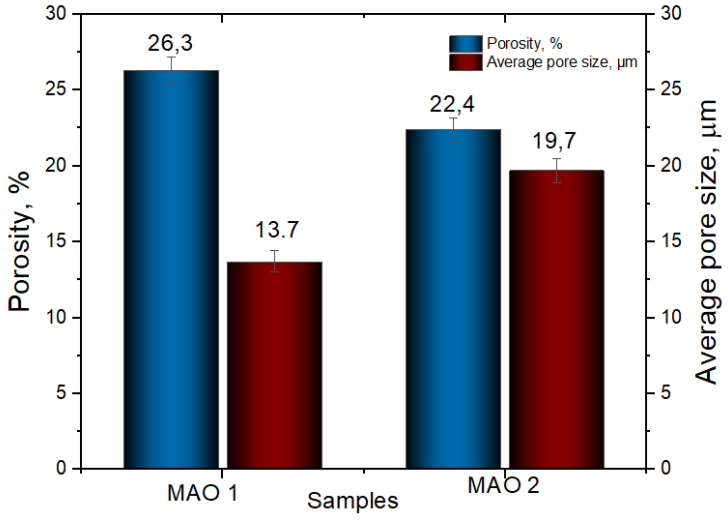

Figure 3. Porosity and average pore size of MAO coatings formed with different TiO_2 nanoparticle concentrations

Figure 3 presents the porosity and average pore-size values of the coatings. For the MAO 1 sample, the total open surface porosity is 26.3 %, with an average pore size of 22.4 μm. Increasing the TiO_2 nanoparticle concentration to 1 % (MAO 2) reduces the open porosity to 13.7 %, while the mean pore size decreases only slightly to 19.7 μm. SEM observations (Fig. 1) show that a few large discharge craters remain visible on MAO 2, but their areal density is lower, so that the overall mean pore diameter is marginally smaller. The reduction in open porosity is attributed to a more intense micro-arc oxidation process and the consequent densification of the oxide layer, which leads to partial closure of discharge channels [38–40]. Although high porosity can facilitate osseointegration by increasing the surface area available for cell attachment, excessive porosity may compromise corrosion resistance and mechanical strength. Thus, a TiO_2 nanoparticle concentration of 1 % promotes the formation of a denser coating with potentially improved structural stability while maintaining the characteristic MAO surface morphology.

Coating Thickness (Cross-Sectional SEM)

Cross-sectional SEM micrographs (Fig. 4) reveal the typical duplex MAO structure with a porous outer layer and a dense inner barrier layer. The coating thickness, determined from three independent measurements on each sample, is about 72±8 μm for MAO 1 and about 123±5 μm for MAO 2. Although no statistical analysis was performed, these values clearly indicate that the coating obtained with 1 wt.% TiO_2 is markedly thicker than the one produced with 0.5 wt.% TiO_2. The increase in thickness can be attributed to the

higher density and energy of micro-discharges in the electrolyte with a larger amount of TiO_2 nanoparticles, which accelerates oxide growth and promotes the formation of a thicker porous layer.

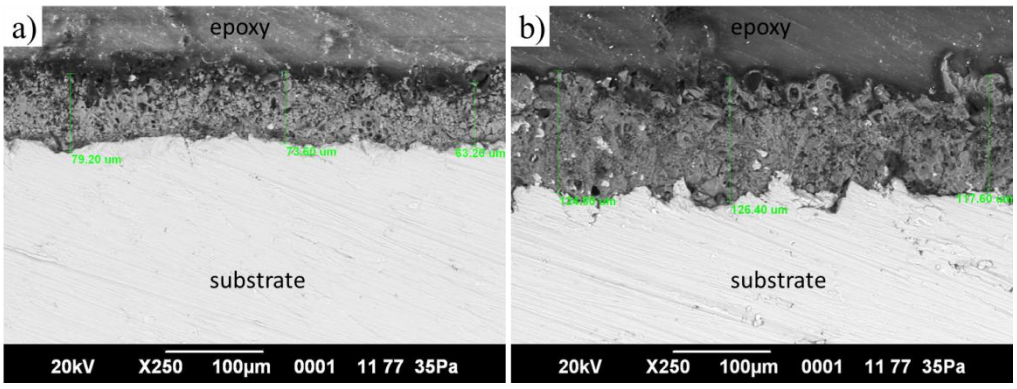

Figure 4. SEM cross-section images of MAO coatings: (*a*) MAO 1, (*b*) MAO 2

A similar increase in coating thickness with a higher TiO_2 content in the electrolyte was also noted in the works [41, 42], where it was shown that TiO_2 nanoparticles increase the conductivity of the electrolyte, enhance the energy of microdischarges and accelerate the growth of the oxide layer.

Surface Roughness

The surface roughness (Ra) values obtained from contact profilometry shown in Figure 5. The untreated titanium surface exhibits an average roughness of 3.55±1.5 µm, which reflects the initial sand-blasted preparation. The TiO_2-free MAO coating (MAO 0) shows a comparable Ra of 3.96±1.2 µm, indicating that the micro-arc oxidation process without nanoparticle additives does not substantially change the macro-scale roughness. In contrast, incorporation of TiO_2 nanoparticles leads to a slight but measurable decrease: MAO 1 — 3.05±0.4 µm and MAO 2 — 2.98±0.7 µm. This trend is consistent with the SEM observations (Figure 1), where the coatings containing nanoparticles display partial closure of large discharge channels and a denser surface. A lower Ra can improve the uniformity of cell attachment while maintaining the characteristic porous microstructure required for osseointegration.

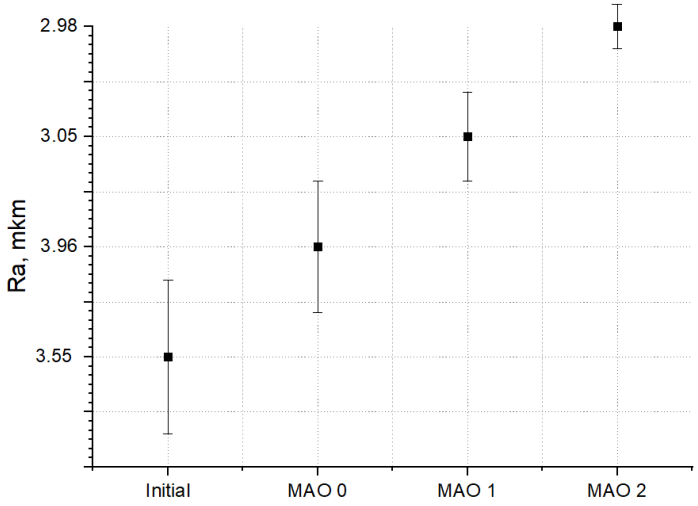

Figure 5. Surface roughness profiles of the tested samples

Corrosion Behavior

The anodic polarization curves (Fig. 6) demonstrate clear differences in the corrosion behavior of bare titanium and MAO-coated samples. In 3.5 wt.% NaCl solution (Figure 6*a*), the corrosion current density (Icorr) of untreated titanium is 1.48×10^{-5} A cm^{-2}, whereas MAO 1 and MAO 2 show markedly lower values of 3.50×10^{-6} A cm^{-2} and 8.89×10^{-6} A cm^{-2}, respectively. Both coatings also exhibit a positive shift of the

corrosion potential, indicating a slowdown of anodic dissolution processes. Among them, the MAO 2 coating provides the most pronounced improvement in the chloride medium. In Ringer's solution (Figure 6*b*), the absolute Icorr values for all samples are lower, reflecting the formation of a protective passive TiO_2 film promoted by the calcium- and phosphate-containing ions of the medium: 2.27×10^{-6} A cm^{-2} for bare titanium, 9.68×10^{-7} A cm^{-2} for MAO 1, and 1.13×10^{-5} A cm^{-2} for MAO 2. Owing to this strong spontaneous passivation, the untreated titanium shows a slightly lower Icorr than the MAO coatings. This effect is well known for titanium in simulated body fluids and represents a temporary passivation phenomenon rather than superior long-term protection. Importantly, in the more aggressive chloride environment (NaCl), the MAO coatings, particularly MAO 2, still provide markedly better protection than bare titanium. The superior corrosion performance of MAO 2 compared with MAO 1 can be attributed to its lower open porosity (13.7 % vs. 26.3 %), which limits the penetration of aggressive ions, and to the higher crystallinity of the oxide layer with an increased content of stable TiO_2 phases [43, 44].

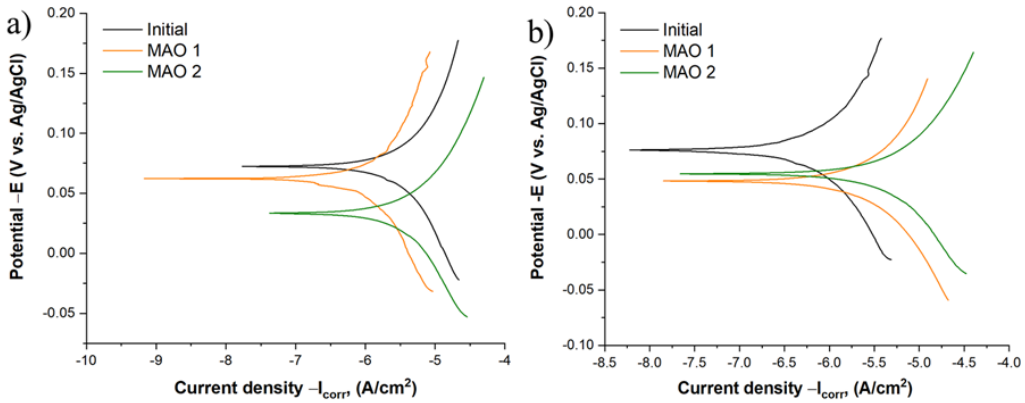

Figure 6. Polarization curves of the samples: (*a*) in 3.5 wt.% NaCl solution; (*b*) in Ringer's solution

Tribological Performance

Figure 7 shows the evolution of the friction coefficient (μ) during ball-on-disk sliding in Ringer's solution.

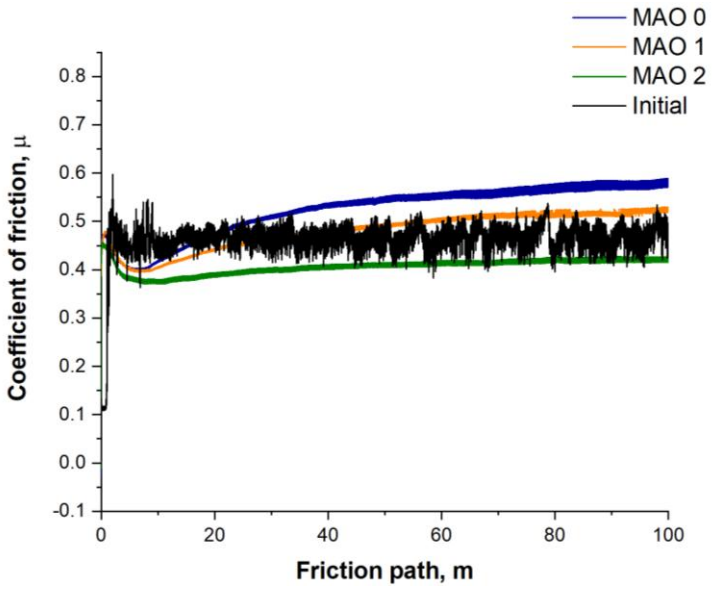

Figure 7. Tribological test results

All samples display an initial running-in stage with a rapid rise in μ, followed by a quasi-steady regime. The untreated titanium and the MAO 0 coating (formed without TiO_2 nanoparticles) exhibit the highest steady-state friction coefficients, stabilizing at about 0.55–0.60 and 0.50–0.55, respectively. For the TiO_2-containing coatings the friction levels are lower overall: MAO 1 reaches approximately 0.46–0.50, while

MAO 2 remains in the range 0.38–0.42 throughout the test. It should be noted that, at longer sliding distances, the μ value of MAO 1 slightly exceeds that of the untreated reference, which we have now stated explicitly; this reflects the combined effect of its relatively high open porosity and the formation of a stable tribolayer rather than any measurement artifact. The progressive reduction of μ from MAO 0 to MAO 2 correlates with the decrease in open surface porosity and the more compact microstructure (Fig. 3), which favor better retention of the lubricating medium and reduce adhesive interactions with the Si_3N_4 counterbody. Thus, the incorporation of TiO_2 nanoparticles, particularly at 1 wt.%, results in coatings with improved tribological behavior compared to both untreated titanium and MAO 0.

In the revised manuscript, Figure 8 presents SEM micrographs of the wear tracks formed after tribological tests in Ringer's solution. The width of the wear scars is approximately 1.2–1.4 mm for all coatings. The MAO 0 surface shows a relatively rough track with visible micro-grooves, typical of abrasive wear. In contrast, MAO 1 and MAO 2 coatings exhibit smoother tracks without signs of delamination, indicating that the oxide layer remained stable under sliding conditions. The MAO 2 sample demonstrates a slightly more compact and uniform wear zone, which correlates with its denser surface structure and lower friction coefficient.

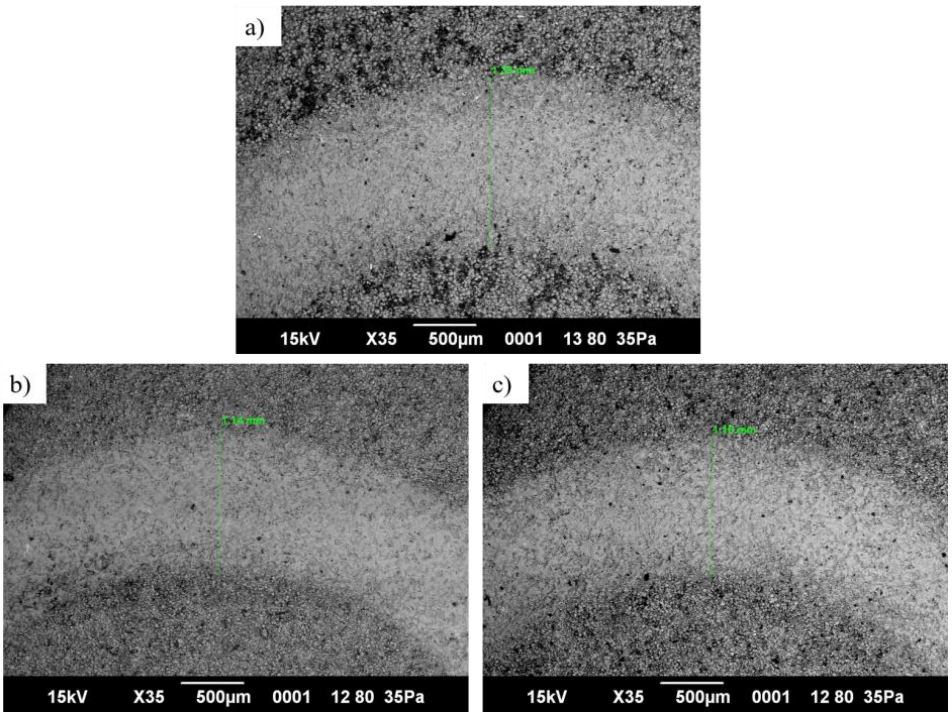

Figure 8. SEM images of wear tracks on the coatings after tribological testing in Ringer's solution:
(*a*) MAO; (*b*) MAO 1; (*c*) MAO 2

Wettability (Water Contact Angle)

Figure 9 shows the static water contact angles of the investigated surfaces. The untreated titanium exhibits a contact angle of 68.0°, corresponding to a weakly hydrophilic surface. After micro-arc oxidation without TiO_2 (MAO 0) the contact angle decreases to 52.0°, and further to 47.2° for MAO 1 (0.5 wt.% TiO_2), indicating a more pronounced hydrophilic character. This trend correlates with the higher surface porosity and the moderately rough topography revealed by SEM and profilometry (Table 1), which favor the capillary penetration of water and thus enhance wetting. For MAO 2 (1 wt.% TiO_2), the contact angle slightly increases to 60.3°, remaining within the hydrophilic range (<90°). The small rise compared with MAO 1 can be related to the lower open porosity (13.7 % vs. 26.3 %) and the denser outer layer, which reduce the capillary effect despite similar Ra values. Overall, all coatings remain hydrophilic, a surface property known to be beneficial for early cell adhesion and subsequent osseointegration of implant materials [45]. All coatings remain hydrophilic (<90°), which is favorable for early cell adhesion.

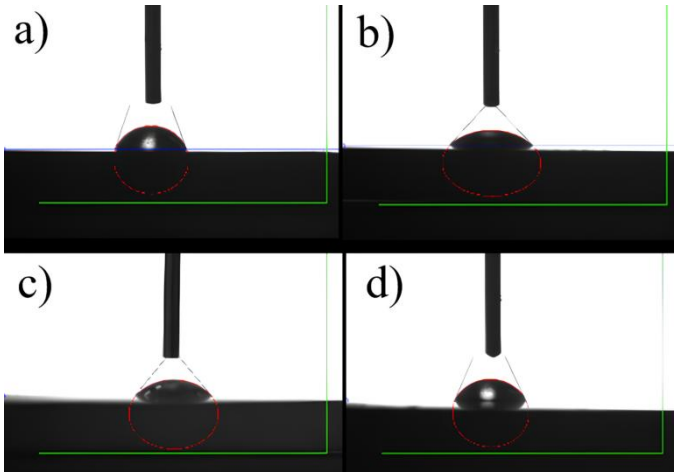

Figure 9. Water contact angle images of the tested surfaces: (*a*) initial, (*b*) MAO 0, (*c*) MAO 1, (*d*) MAO 2

Cytotoxicity and Surface Stability in Cell Culture

In this study, dark-field light microscopy was employed to assess the microrelief of the coating surfaces before and after thermal sterilization, as well as to analyze the uniformity and structural changes induced by technological treatments. Reflective dark-field microscopy of the samples (Fig. 10) revealed a pronounced microrelief typical of calcium–phosphate coatings formed by the micro-arc oxidation process, consisting of bright spherulitic structures and darker surface depressions.

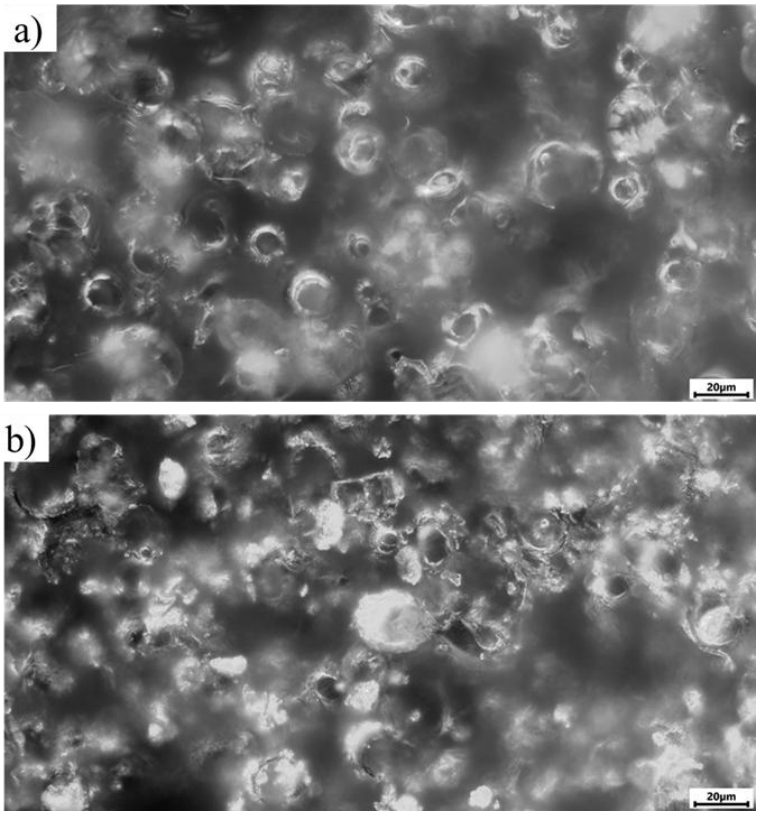

Figure 10. Microscopic appearance of the sample surfaces before dry-heat sterilization (dark-field light microscopy), magnification ×500; (*a*) sample No. 31 from the MAO 1 group; (*b*) sample No. 21 from the MAO 2 group

After sterilization at 160 °C for 60 min (prior to contact with the liquid cell culture), no additional surface integrity changes (such as cracks or delamination of structural elements) were observed. However, when the sterile samples were placed in the cell suspension, yellowing of the culture medium was noticeable in the MAO 2 group (Fig. 11). Only sample No. 25 displayed a medium color similar to that of the control group

(cells without samples, K1 for comparison) and the MAO 1 test group (sample No. 35 for comparison). In addition, a white amorphous, flake-like precipitate formed at the bottom of the test tubes containing samples No. 21–24 (MAO 2 group), which was absent in the control tubes and in tubes containing samples No. 25 and No. 35. Synthetic cell culture media have their own buffering systems that protect against pH fluctuations. The yellowing observed in group 2 indicates acidification of the medium caused by chemical products released from the samples (e.g., detachment of structural coating elements or residual products of the micro-arc oxidation process that were not fully removed during sample preparation). pH fluctuations of ±1 unit from the neutral range (7.0–7.4) indicate that the sample did not pass sanitary-chemical suitability tests for potential implant use. Therefore, samples from the MAO 2 group may subsequently demonstrate excessive cytotoxicity in the MTT assay.

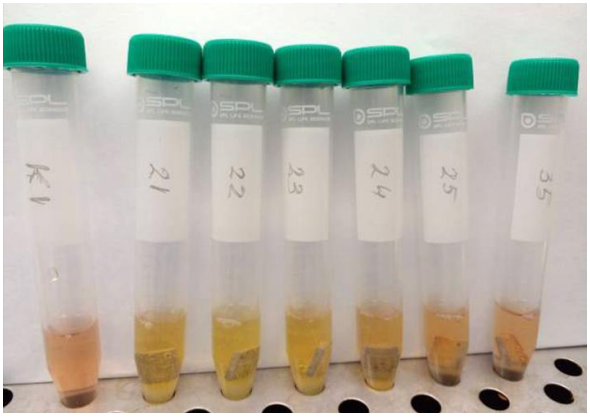

Figure 11. Change in the color of the culture medium immediately after adding samples from the MAO 2 group (Nos. 21–24)

In this context, it should be noted that after contact with the cell culture, coating defects were observed on both sides of the MAO 2 samples, particularly along the edges, which may indicate partial dissolution of the coating and precipitation of its components into the medium (Fig. 10). In the MAO 1 group, this effect was much less pronounced. Edge defects of MAO coatings have been reported in the literature in cases of excessive coating dissolution and are presumably associated with "stress concentrators." The condition of a normal distribution of sample characteristics was not met; therefore, a nonparametric test was used to compare the results between the MAO 1 and MAO 2 groups. Verification according to Section 2.1.1 of the PI guidelines (Table 1) showed that the median cytotoxicity index (CI) in the MAO 2 group significantly exceeded the 30 % in vitro cytotoxicity threshold recommended by ISO 10993-5, reaching 81 % cell death compared to the control. In contrast, the MAO 1 group had a median CI of 3 % (Table 2), indicating the non-cytotoxic nature of the samples in this group. Statistically significant differences (p<0.001) in the median CI values were identified between the two groups (Table 3).

Table 1

Verification of MTT test results for the normal distribution of variables in the studied samples

Group	Shapiro–Wilk Test with Royston's Correction	Normal Distribution Law of the Variable
MAO 1	SW = 0.94, p = 0.13	yes
MAO 2	SW = 0.66, p < 0.001	no

Table 2

Intergroup comparison of MTT test results in the studied samples

Group	Cytotoxicity Index Values, % of Control, Me (Q1; Q3)	Pairwise Comparison, Brunner–Munzel Test
MAO 1	3 (−2; 10)	Brunner–Munzel Test Statistic = 17.63 p < 0.001
MAO 2	81 (76; 84)	

Thus, the MAO 2 group samples exhibit a significant cytotoxic effect (>30 % relative to control) on the in vitro culture of HOS human osteosarcoma cells under direct short-term contact for 24 h. The results presented in Tables 3 and 4 indicate that the cytotoxic effect in the MAO 1 group varies around zero. Notably, sample No. 32 demonstrates statistically significant differences from the other samples in this group, showing a cytoprotective effect (enhanced cell viability).

Table 3

Intragroup comparison of MTT test results among samples within the MAO 1 group

Group	Cytotoxicity Index Values, % of Control (X ± SD)	Multiple Comparison, Welch's ANOVA	Pairwise Comparison, Games–Howell Test
Sample 31	10 ± 7	F = 7.21 p = 0.0054*	$p_{31–32}$ = 0.0067* $p_{31–33}$ = 0.99 $p_{31–34}$ = 0.28 $p_{31–35}$ = 0.99 $p_{32–33}$ = 0.0091* $p_{32–34}$ = 0.099 $p_{32–35}$ = 0.0095 $p_{33–34}$ = 0.39 $p_{33–35}$ = 0.99 $p_{34–35}$ = 0.41
Sample 32	−15.80 ± 8.82		
Sample 33	8.80 ± 7.19		
Sample 34	−0.2 ± 7.82		
Sample 35	8.6 ± 7.16		
* n — sample size (number of measurement replicates); the intragroup distribution of the variable was consistent with normality according to the Shapiro–Wilk test with Royston's correction.			

In turn, with the exception of sample No. 25 (CI = 11.8 %), the remaining four samples showed CI values in the range of 77.0 %–90.8 % (Table 4), which is 2.5–3 times higher than the threshold level recommended by ISO 10993-5 (not exceeding 30 %).

Table 4

Intragroup comparison of MTT test results among samples within the MAO 2 group

Group	n	Cytotoxicity Index Values, % of Control (X ± SD)	Multiple Comparison, Welch's ANOVA	Pairwise Comparison, Games–Howell Test
Sample 21	5	80.60 ± 1.67	F = 201.47 p < 0.001*	$p_{21–22}$ < 0.001* $p_{21–23}$ = 0.042* $p_{21–24}$ = 0.071 $p_{21–25}$ < 0.001* $p_{22–23}$ < 0.001* $p_{22–24}$ < 0.001* $p_{22–25}$ < 0.001* $p_{23–24}$ = 0.0014* $p_{23–25}$ < 0.001* $p_{24–25}$ < 0.001*
Sample 22	5	90.80 ± 0.84		
Sample 23	5	84 ± 1.23		
Sample 24	5	77 ± 1.87		
Sample 25	5	11.80 ± 6.61		
* n — sample size (number of measurement replicates); the intragroup distribution of the variable was consistent with normality according to the Shapiro–Wilk test with Royston's correction.				

Microscopic imaging of the sample surfaces after Azure II/eosin staining was used to visualize HOS cells adhered to the coatings (Fig. 12). Because of the irregular microrelief and variable depth of the MAO surface it was not possible to obtain sharply focused micrographs at all sites, even at low magnification (×200). Nevertheless, representative low-magnification images of the MAO 1 group (Fig. 12*a*) show multiple scattered stained areas corresponding in size to individual cells. Examination of several fields of view at higher magnification (×500) confirmed the presence of cell nuclei-like structures in these stained regions (Fig. 12*b*). For the MAO 2 group (Fig. 12*c*), stained elements were also found, but in repeated fields the overall number of attached cells was lower than on MAO 1, even though the single representative image shows two stained spots. The lower apparent count in the selected micrographs should therefore be interpreted qualitatively; the conclusion of higher cell adhesion on MAO 1 is based on observation of multiple areas rather than only the frames shown.

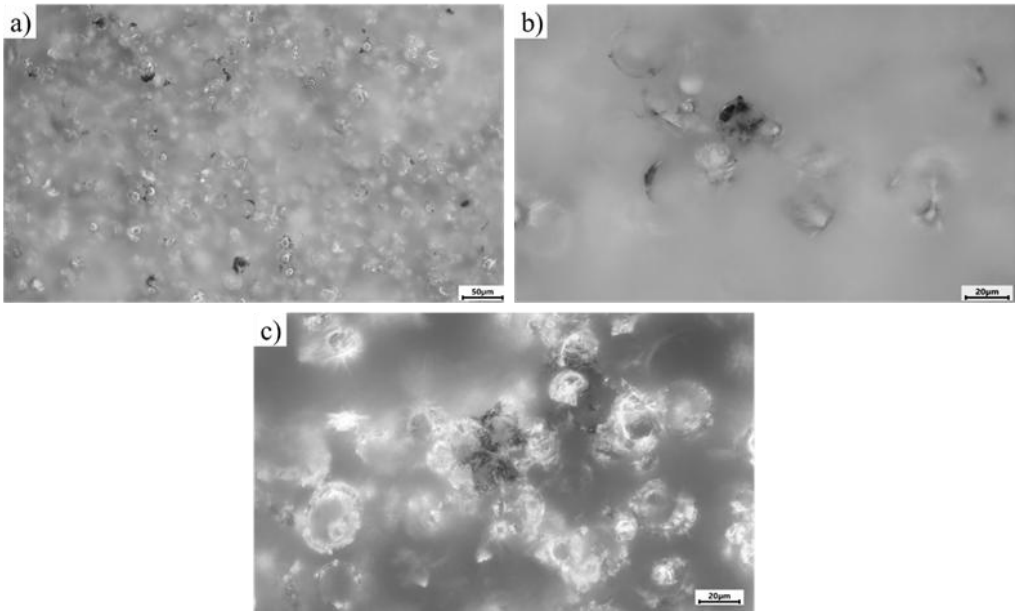

(*a*) MAO 1 No. 33, dark-field, ×200: numerous stained regions corresponding in size to individual cells are visible across the surface; (*b*) MAO 1, bright-field, ×500: single stained element showing a cell-nucleus-like structure; (*c*) MAO 2 No. 22, dark-field, ×500: representative view with two stained elements

Figure 12. Microscopic appearance of sample surfaces after 24 h contact with HOS cells and Azure II/eosin staining

Figure 12 presents the SEM results of the samples after cytotoxicity testing. For the MAO 1 group samples (Fig. 12*a*, *b*), the surface largely retains its original coating structure with minimal signs of degradation. The morphology remains relatively stable, with individual areas showing adhered cellular elements, confirming the low cytotoxicity of the coating and its ability to support cell adhesion. No significant dissolution or delamination of the coating was observed. In contrast, the MAO 2 group samples (Fig. 12*c*, *d*) exhibit more pronounced coating degradation, including localized dissolution, the appearance of microcracks, and areas where structural elements have delaminated. Some regions display residual decomposition products of the coating, likely released into the culture medium, correlating with the color change observed at the early stages of the experiment (Fig. 11). Such surface alterations indicate coating instability and potential release of particles or ions that may cause toxic effects on cells [46–50].

The higher cytotoxicity observed for the MAO 2 coating containing 1 wt.% TiO_2 may be related to several factors. First, a higher TiO_2 concentration can alter the electrolyte chemistry during coating growth and subsequently affect the surface stability in the biological medium. Partial leaching of Ti and P ions and local pH fluctuations may occur, leading to unfavorable conditions for cell viability. In addition, the increased discharge energy and the formation of a thicker, more porous layer can promote partial structural degradation and enhanced release of reaction products into the culture medium. Similar effects were reported by other authors for oxide coatings obtained at high nanoparticle concentrations.

EDS elemental mapping and spectra (Fig. 13) confirm the presence of titanium, calcium, phosphorus, oxygen, and trace amounts of carbon in both coatings. In the MAO 1 sample (non-cytotoxic coating), the distribution of calcium and phosphorus remains relatively uniform across the surface, and the overall composition shows minimal changes after contact with the cell culture. This indicates good chemical stability of the coating and low release of degradation products into the surrounding medium, correlating with the absence of cytotoxic effects. In contrast, the MAO 2 sample exhibits decreased phosphorus and calcium signals accompanied by an increased titanium and oxygen contribution, suggesting partial dissolution of the calcium–phosphate layer and exposure of the underlying titanium oxide phase. These compositional changes are consistent with the previously observed yellowing of the culture medium and the higher cytotoxicity index (>30 %). Thus, coatings formed with 0.5 % TiO_2 nanoparticles (MAO 1) demonstrate better chemical stability and biocompatibility compared to coatings formed with 1 % TiO_2 (MAO 2).

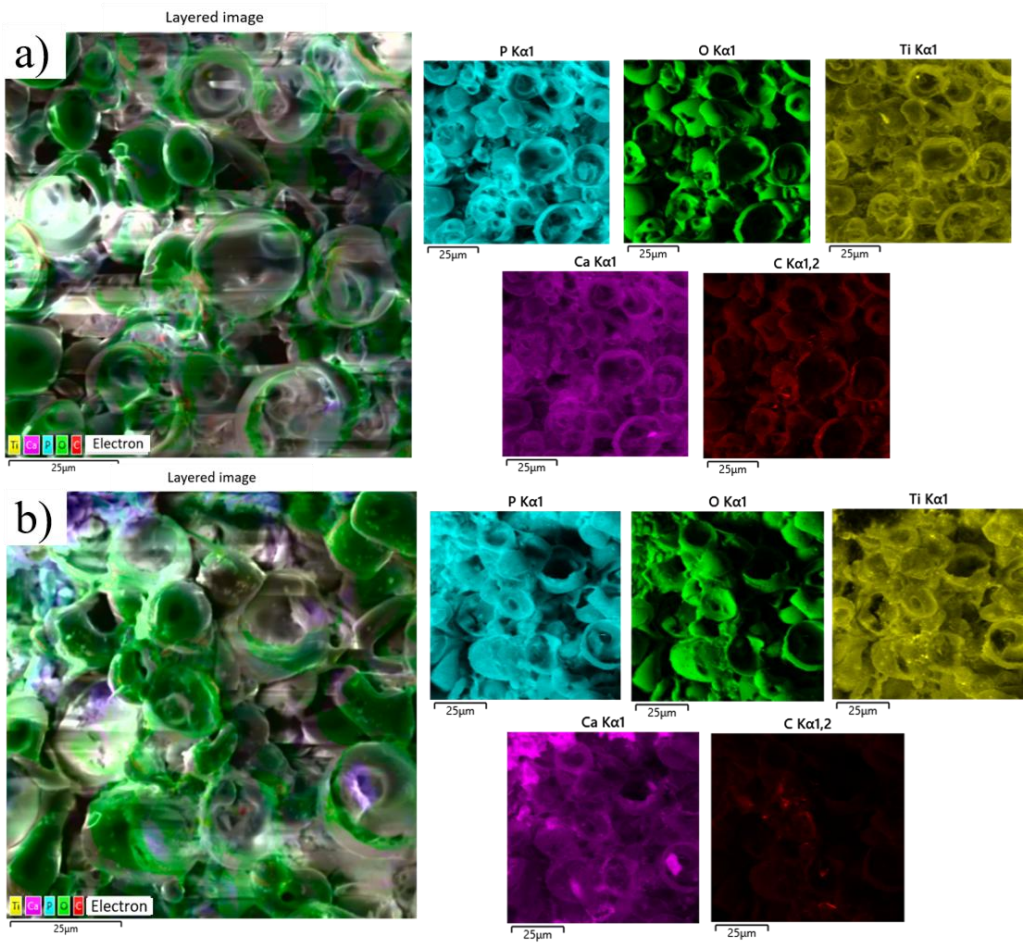

Figure 13. EDS analysis of MAO coatings after cytotoxicity testing: (*a*) MAO 1; (*b*) MAO 2

Table 5 summarizes the elemental composition of the coatings obtained from EDS mapping. Both coatings consist primarily of oxygen, phosphorus, and calcium, confirming the formation of a calcium–phosphate–titania layer. The titanium content is about 10.17 wt.% in MAO 1 and 7.24 wt.% in MAO 2, indicating that TiO_2 nanoparticles are successfully incorporated into the oxide layer. The slightly lower Ti content at 1 wt.% TiO_2 addition is consistent with the thicker Ca–P-rich outer layer and agrees with the XRD identification of anatase and rutile phases. These EDS results, together with the XRD and SEM analyses, confirm the presence and stable incorporation of TiO_2 nanoparticles in the MAO coatings.

Table 5

Elemental composition (EDS, weight %) of the MAO coatings

Element MAO 1	Weight, %	Element MAO 2	Weight, %
O	38.24	O	41.72
P	30.12	P	23.68
Ti	10.17	Ti	7.24
Ca	15.31	Ca	20.18
C	6.16	C	7.18

The observed differences between coatings produced with 0.5 and 1 wt.% TiO_2 nanoparticles can be explained by the influence of nanoparticle concentration on the micro-arc discharge behavior and the kinetics of oxide growth. TiO_2 nanoparticles in the electrolyte act as additional charge carriers and heterogeneous nucleation sites, which modify the breakdown voltage and increase the density and energy of micro-discharges [51]. At a higher nanoparticle content (1 wt.%), the higher discharge energy promotes more intense local melting and resolidification of the oxide, leading to partial closure of discharge channels and formation of a denser, more crystalline TiO_2-containing layer. Conversely, at 0.5 wt.%, the lower concentration

of particles results in a more open, highly porous structure with larger areal density of discharge craters. These microstructural changes directly affect the corrosion behavior, tribological performance, and cytotoxicity of the coatings.

Conclusion

This study demonstrated that the incorporation of TiO_2 nanoparticles into the electrolyte during micro-arc oxidation significantly affects the morphology, phase composition, and functional characteristics of calcium–phosphate coatings formed on titanium. Both coatings exhibited a typical duplex structure with a porous outer layer and a dense inner barrier layer. Increasing the TiO_2 content from 0.5 wt.% to 1 wt.% resulted in a thicker coating (from 72±8 μm to 123±5 μm) and a higher proportion of anatase and rutile phases, which influenced the mechanical and electrochemical performance.

The coating produced with 0.5 wt.% TiO_2 (MAO 1) demonstrated a uniform microstructure, improved corrosion resistance, and the absence of cytotoxic effects, making it the most balanced composition in terms of protective and biological performance. In contrast, the coating with 1 wt.% TiO_2 (MAO 2) exhibited partial degradation and elevated cytotoxicity, likely caused by pH changes and ion release into the biological medium.

The developed coatings show strong potential for application on biomedical titanium implants, particularly for orthopedic and dental devices, where corrosion stability, surface bioactivity, and cell compatibility are critical. The MAO 1 coating, in particular, may serve as a bioactive and corrosion-resistant layer that enhances implant longevity and integration with bone tissue.

Future research will focus on long-term in vitro and in vivo testing to evaluate the coatings' osteogenic properties and biological stability, as well as on optimizing the MAO parameters and electrolyte composition to achieve an improved balance between coating thickness, porosity, and bioactivity. Additional attention will be given to ion-leaching behavior, mechanical fatigue resistance, and coating adhesion under dynamic physiological conditions to ensure the reliability of these coatings in real biomedical applications.

Funding

This research has been funded by the Committee of Science of the Ministry of Science and Higher Education of the Republic of Kazakhstan (Grant No. BR24992862).

References

1 Akshaya, S., Rowlo, P.K., Dukle, A., & Nathanael, A.J. (2022). Antibacterial coatings for titanium implants: Recent trends and future perspectives. *Antibiotics, 11,* 1719. https://doi.org/10.3390/antibiotics11121719

2 Besisa, N.H.A., & Yajima, T. (2024). Titanium-Based Alloys: Classification and Diverse. *Titanium-Based Alloys — Characterization and Applications,* 125.

3 Spriano, S., Yamaguchi, S., Baino, F., & Ferraris, S. (2018). A critical review of multifunctional titanium surfaces: New frontiers for improving osseointegration and host response, avoiding bacteria contamination. *Acta Biomaterialia, 79,* 1–22. https://doi.org/10.1016/j.actbio.2018.08.013

4 Liu, Z., Liu, X., & Ramakrishna, S. (2021). Surface engineering of biomaterials in orthopedic and dental implants: Strategies to improve osteointegration, bacteriostatic and bactericidal activities. *Biotechnology Journal, Vol. 16,* 2000116. https://doi.org/10.1002/biot.202000116

5 Kengesbekov, A.B., Serikbaykyzy, A., Bayandinova, M.B., Batanov E.E., Bazarov N.E., & Askhatov A.N. (2025). Development of biocompatible coatings for orthopedic joint implants. *Physical Sciences and Technology, 12,* 84–94. https://doi.org/10.26577/phst20251218

6 Ben Arbia, M., Helal, H., & Comini, E. (2024). Recent advances in low-dimensional metal oxides via sol-gel method for gas detection. *Nanomaterials, 14,* 359. https://doi.org/10.3390/nano14040359

7 Prasad, K.N., Syed, I., & Subbu, S.K. (2022). Laser dimple texturing — applications, process, challenges, and recent developments: A review. *Australian Journal of Mechanical Engineering, 20,* 316–331. https://doi.org/10.1080/14484846.2019.1705533

8 Roccaforte, F., Giannazzo, F., & Greco, G. (2022). Ion implantation doping in silicon carbide and gallium nitride electronic devices. *Micro, 2,* 23–53. https://doi.org/10.3390/micro2010002

9 Xie, J., Zhang, C., & Waite, T.D. (2022). Hydroxyl radicals in anodic oxidation systems: Generation, identification and quantification. *Water Research, 217,* 118425. https://doi.org/10.1016/j.watres.2022.118425

10 Xue, T., Attarilar, S., Liu, S., Liu, J., Song, X., Li, L., & Tang, Y. (2020). Surface modification techniques of titanium and its alloys to functionally optimize their biomedical properties: Thematic review. *Frontiers in Bioengineering and Biotechnology, 8,* 603072. https://doi.org/10.3389/fbioe.2020.603072

11 Alontseva, D., Safarova, Y., Voinarovych, S., Obrosov, A., Yamanoglu, R., Khoshnaw, F., & Weiß, S. (2024). Biocompatibility and corrosion of microplasma-sprayed titanium and tantalum coatings versus titanium alloy. *Coatings, 14,* 206. https://doi.org/10.3390/coatings14020206

12 Zhang, Z.Y., Huang, T.Y., Zhai, D.J., Wang, H.B., Feng, K.Q., & Xiang, L. (2022). Study on strontium doped bioactive coatings on titanium alloys surfaces by micro-arc oxidation. *Surface and Coatings Technology, 451,* 129045. https://doi.org/10.1016/j.surfcoat.2022.129045

13 Wen, X., Liu, Y., Xi, F., Zhang, X., & Kang, Y. (2023). Micro-arc oxidation (MAO) and its potential for improving the performance of titanium implants in biomedical applications. *Frontiers in Bioengineering and Biotechnology, 11,* 1282590. https://doi.org/10.3389/fbioe.2023.1282590

14 Wang, R., Ni, S., Ma, L., & Li, M. (2022). Porous construction and surface modification of titanium-based materials for osteogenesis: A review. *Frontiers in Bioengineering and Biotechnology, 10,* 973297. https://doi.org/10.3389/fbioe.2022.973297

15 Manisekaran, R., Chettiar, A.D.R., Marasamy, L., Arthikala, M.K., Kandasamy, G., Ibarra, V.C., & Rathore, H.S. (2025). Copper, Zinc, and Titanium-Based Semiconductor Nanomaterials for Antimicrobial Coatings and Their Mechanisms. *Nano Select, 6,* e202400155. https://doi.org/10.1002/nano.202400155

16 Rezić, I., & Meštrović, E. (2023). Characterization of nanoparticles in antimicrobial coatings for medical applications — a review. *Coatings, 13,* 1830. https://doi.org/10.3390/coatings13111830

17 Parham, S., Wicaksono, D.H., Bagherbaigi, S., Lee, S.L., & Nur, H. (2016). Antimicrobial treatment of different metal oxide nanoparticles: A critical review. *Journal of the Chinese Chemical Society, 63,* 385–393. https://doi.org/10.1002/jccs.201500446

18 Vera, M.L., Traid, H.D., Dwojak, A.N., Rosenberger, M.R., & Schvezov, C.E. (2023). Advances in nanostructured TiO_2 coatings for industrial applications. In *Industrial Applications of Nanoparticles* (pp. 228–255). CRC Press: Boca Raton, FL, USA. https://doi.org/10.1201/9781003183525

19 Rakhadilov, B., Zhassulan, A., Ormanbekov, K., Shynarbek, A., Baizhan, D., & Aldabergenova, T. (2024). Surface modification and tribological performance of calcium phosphate coatings with TiO_2 nanoparticles on VT1-0 titanium by micro-arc oxidation. *Crystals, 14,* 945. https://doi.org/10.3390/cryst14110945

20 Kengesbekov, A., Sagdoldina, Z., Torebek, K., Baizhan, D., Kambarov, Y., Yermolenko, M., & Maulet, M. (2022). Synthesis and formation mechanism of metal oxide compounds. *Coatings, 12,* 1511. https://doi.org/10.3390/coatings12101511

21 Abbasi-Oshaghi, E., Mirzaei, F., & Pourjafar, M. (2019). NLRP3 inflammasome, oxidative stress, and apoptosis induced in the intestine and liver of rats treated with titanium dioxide nanoparticles: In vivo and in vitro study. *International Journal of Nanomedicine, 14,* 1919–1936. https://doi.org/10.2147/IJN.S192382

22 Kumar, V., Sharma, N., & Maitra, S.S. (2017). In vitro and in vivo toxicity assessment of nanoparticles. *International Nano Letters, 7,* 243–256. https://doi.org/10.1007/s40089-017-0221-3

23 Ajdary, M., Moosavi, M.A., Rahmati, M., Falahati, M., Mahboubi, M., Mandegary, A., & Varma, R.S. (2018). Health concerns of various nanoparticles: A review of their in vitro and in vivo toxicity. *Nanomaterials, 8,* 634. https://doi.org/10.3390/nano8090634

24 Salama, B., Alzahrani, K.J., Alghamdi, K.S., Al-Amer, O., Hassan, K.E., Elhefny, M.A., & Fathalla, A.S. (2023). Silver nanoparticles enhance oxidative stress, inflammation, and apoptosis in liver and kidney tissues: Potential protective role of thymoquinone. *Biological Trace Element Research, 201,* 2942–2954. https://doi.org/10.1007/s12011-022-03399-w

25 Zhang, X., Zhou, W., Xi, W. (2024). Advancements in incorporating metal ions onto the surface of biomedical titanium and its alloys via micro-arc oxidation: A research review. *Frontiers in Chemistry, 12,* 1353950. https://doi.org/10.3389/fchem.2024.1353950

26 Xu, N., Fu, J., Zhao, L., Chu, P.K., & Huo, K. (2020). Biofunctional elements incorporated nano/microstructured coatings on titanium implants with enhanced osteogenic and antibacterial performance. *Advanced Healthcare Materials, 9,* 2000681. https://doi.org/10.1002/adhm.202000681

27 Ming, X., Wu, Y., Zhang, Z., & Li, Y. (2023). Micro-arc oxidation in titanium and its alloys: Development and potential of implants. *Coatings, 13,* 2064. https://doi.org/10.3390/coatings13122064

28 Rakhadilov, B., Zhassulan, A., Baizhan, D., Shynarbek, A., Ormanbekov, K., & Aldabergenova, T. (2024). The effect of the electrolyte composition on the microstructure and properties of coatings formed on a titanium substrate by microarc oxidation. AIMS *Materials Science, 11,* 547–564. https://doi.org/10.3934/matersci.2024027

29 Bayatanova, L.B., Zhassulankyzy, A.Z., Magazov, N.M., Rakhadilov, B.K., Muktanova, N., & Uazyrkhanova, G.K. (2023). Effect of plasma-electrolytic oxidation on mechanical properties of titanium coatings. *Bulletin of the University of Karaganda-Physics, 111,* 65–74. https://doi.org/10.31489/2023ph3/65-74

30 Kashin, A.D., Sedelnikova, M.B., Uvarkin, P.V., Ugodchikova, A.V., Luginin, N.A., Sharkeev, Y.P., & Bakina, O.V. (2023). Functionalizing diatomite-based micro-arc coatings for orthopedic implants: Influence of TiO_2 addition. *Biomimetics, 8,* 280. https://doi.org/10.3390/biomimetics8030280

31 Makurat-Kasprolewicz, B., Wekwejt, M., Ronowska, A., Gajowiec, G., Grodzicka, M., Dzionk, S., & Ossowska, A. (2024). Influence of ultrasound on the characteristics of CaP coatings generated via the micro-arc oxidation process in relation to biomedical engineering. *ACS Biomaterials Science & Engineering, 10,* 2100–2115. https://doi.org/10.1021/acsbiomaterials.3c01433

32 (2009). ISO 10993-5. Biological Evaluation of Medical Devices — Part 5: Tests for *In Vitro* Cytotoxicity. Geneva: International Organization for Standardization.

33 Wang, P., Wei, X.W., Cao, W.J., Tang, Y.T., Wang, Y., Gong, Z.Y., & Zu, X.T. (2019). Effect of TiO_2 nanoparticles on the characteristics of MAO coatings. *International Journal of Electrochemical Science, 14,* 9311–9325. https://doi.org/10.20964/2019.09.67

34 Woo, S.R., & Sung, Y.M. (2016). Enhanced photoelectrochemical water splitting of micro-arc oxidized TiO_2 via anatase/rutile phase control and nitrogen doping. *Journal of the Electrochemical Society, 163,* H278. https://doi.org/10.1149/2.0471605jes

35 Yerokhin, A.L., Nie, X., Leyland, A., & Matthews, A. (2000). Characterization of oxide films produced by plasma electrolytic oxidation of a Ti–6Al–4V alloy. *Surface and Coatings Technology, 130,* 195–206. https://doi.org/10.1016/S0257-8972(00)00719-2

36 Ceriani, F., Casanova, L., Massimini, L., Brenna, A., & Ormellese, M. (2023). TiO_2 microparticles incorporation in coatings produced by plasma electrolytic oxidation (PEO) on Titanium. *Coatings, 13,* 1718. https://doi.org/10.3390/coatings13101718

37 Erfanifar, E., Aliofkhazraei, M., Nabavi, H.F., & Rouhaghdam, A.S. (2017). Growth kinetics and morphology of microarc oxidation coating on titanium. *Surface and Coatings Technology, 315,* 567–576. https://doi.org/10.1016/j.surfcoat.2017.03.002

38 Zhang, P., Zuo, Y., & Nie, G. (2020). The pore structure and properties of microarc oxidation films on 2024 aluminum alloy prepared in electrolytes with oxide nanoparticles. *Journal of Alloys and Compounds, 816,* 152520. https://doi.org/10.1016/j.jallcom.2019.152520

39 Jin, F., Chu, P.K., Tong, H., & Zhao, J. (2006). Improvement of surface porosity and properties of alumina films by incorporation of Fe micrograins in micro-arc oxidation. *Applied Surface Science, Vol. 253,* 863–868. https://doi.org/10.1016/j.apsusc.2006.01.024

40 Li, Z., Cai, Z.B., Cui, X.J., Liu, R.R., Yang, Z.B., & Zhu, M.H. (2021). Influence of nanoparticle additions on structure and fretting corrosion behavior of micro-arc oxidation coatings on zirconium alloy. *Surface and Coatings Technology, Vol. 410,* 126949. https://doi.org/10.1016/j.surfcoat.2021.126949

41 Bayatanova, A.M., Rakhadilov, B.K., & Abizhanova, I.K., et al. (2023). Effect of plasma-electrolytic oxidation on mechanical and corrosion properties of titanium coatings with TiO_2 nanoparticles. *Bulletin of the University of Karaganda-Physics, 3*(111), 54–61. https://doi.org/10.31489/2023ph3/65-74

42 Molaei, M., Bahrololoom, M.E., & Heshmati-Manesh, S., et al. (2022). Incorporating TiO_2 nanoparticles to enhance corrosion resistance and bioactivity of micro-arc oxidized titanium coatings. *Ceramics International, 48, 15,* 22021–22031. DOI: 10.1016/j.ceramint.2022.06.149

43 Kumar, K., Bhadauria, S.S., & Singh, A.P. (2023). Effect of post-coating heat treatment on corrosion and stress corrosion behaviors of NiCr/TiO_2-coated 316L stainless steel. *Arabian Journal of Science and Engineering, 48,* 3893–3908. https://doi.org/10.1007/s13369-022-07310-6

44 Chen, X.W., Song, H., Pu, H., Zheng, R., Zhang, M., & Zhang, D. (2024). Study of wear and corrosion resistance of ATO nanoparticle–doped micro-arc oxide film layers. *International Journal of Applied Ceramic Technology, 21,* 1078–1093. https://doi.org/10.1111/ijac.14599

45 Steel, J.P. (1927). The treatment of certain mental diseases by Ringer-Locke solution. *British Medical Journal, 2,* 1177. https://doi.org/10.1136/bmj.2.3494.1177

46 Suthar, J.K., Rakesh, B., Vaidya, A., & Ravindran, S. (2023). Comprehensive analysis of titanium oxide nanoparticle size and surface properties on neuronal PC-12 cells: Unraveling cytotoxicity, dopaminergic gene expression, and acetylcholinesterase inhibition. *Journal of Xenobiotics, 13,* 662–684. https://doi.org/10.3390/jox13040043

47 Line, F.C. (2023). Titanium dioxide nanoparticle (TiO_2 NP) induces toxic effects on LA-9 mouse fibroblast cell line. *Cellular Physiology and Biochemistry, 57,* 63–81. https://doi.org/10.33594/000000616

48 Mohammadalipour, Z., Rahmati, M., Khataee, A., & Moosavi, M.A. (2017). Different concentrations of titanium dioxide nanoparticles induce autophagy followed by growth inhibition or cell death in A375 melanoma cells. *Journal of Skin Stem Cell, 4,* e63994. https://doi.org/10.5812/jssc.63994

49 Jin, C.Y., Zhu, B.S., Wang, X.F., & Lu, Q.H. (2008). Cytotoxicity of titanium dioxide nanoparticles in mouse fibroblast cells. *Chemical Research in Toxicology, Vol. 21,* 1871–1877. https://doi.org/10.1021/tx800179f

50 Zhu, G., Wang, G., & Li, J.J. (2021). Advances in implant surface modifications to improve osseointegration. *Materials Advances, 2,* 6901–6927. https://doi.org/10.1039/D1MA00675D

51 Mamaeva, A., Kenzhegulov, A., Panichkin, A., Abdulvaliyev, R., Fischer, D., Bakhytuly, N., & Toiynbaeva, N. (2024). Influence of current duty cycle and voltage of micro-arc oxidation on the microstructure and composition of calcium phosphate coating. *Coatings, 14,* 766. https://doi.org/10.3390/coatings14060766

А.Б. Кеңесбеков, А.Ж. Жасұлан, Н. Мұқтанова,
Дарын Байжан, Е. Ахметова, А. Серікбайқызы

Титандағы РЕО-кальций-фосфаты жабындарының коррозияға төзімділігін, цитоүйлесімділігін және бактерияға қарсы қасиеттерін арттыру үшін TiO_2 нанобөлшектерін енгізу

Титан және оның қорытпалары қолайлы механикалық қасиеттеріне және коррозияға төзімділігіне байланысты биомедициналық имплантацияларда кеңінен қолданылады; дегенмен, олардың табиғи бетінде жеткілікті биобелсенділік пен бактерияға қарсы қасиеттері жоқ. Микродоғалық тотығу биоактивті жабындарды өндірудің перспективалы тәсілі және TiO_2 сияқты нанобөлшектердің қосылуы олардың функционалдығын одан әрі жақсартуы мүмкін. Бұл зерттеу жабын тұрақтылығы мен биологиялық қауіпсіздікті қамтамасыз ететін микродоғалық тотығу электролитіндегі TiO_2 нанобөлшектерінің оңтайлы концентрациясын анықтауға бағытталған. Кальций-фосфатты жабындар екі TiO_2 концентрациясы бар микродоғалық тотығу арқылы коммерциялық таза титанда дайындалды: 0,5 % масса (МАО 1) және 1 % масса (МАО 2). Беттің морфологиясы, кеуектілігі және фазалық құрамы сканерлеуші электрондық микроскопия, энергия-дисперсиялық спектроскопия және рентген сәулелерінің дифракциясы арқылы талданды. Коррозияға төзімділік NaCl және Рингер ерітінділеріндегі потенциодинамикалық поляризация арқылы бағаланды, ал биоүйлесімділік HOS адам остеосаркома жасушалары мен МТТ талдаулары арқылы *in vitro* арқылы бағаланды. TiO_2 мазмұнын 1 %-ға ұлғайту жабынның кеуектілігін төмендетті (МАО 1 үшін 13,7 %-ға қарсы 26,3 %), коррозиядан қорғауды жақсартты және жалаң титанмен салыстырғанда үйкеліс коэффициентін төмендетті. Дегенмен МАО 2 биологиялық ортада жоғары цитотоксикалық (81 % жасуша өлімі) және ішінара құрылымдық деградацияны көрсетті. МАО 1 тұтастығын сақтап, уытты әсерлерін көрсетпеді (3 % жасуша өлімі). Бұл нәтижелер TiO_2 0,5 %-нің коррозияға төзімділік, механикалық тұрақтылық және биоүйлесімділік арасындағы тепе-теңдікті қамтамасыз ете отырып, қауіпсіз имплант жабындарының дамуын қолдайтын оңтайлы концентрация екенін көрсетеді.

Кілт сөздер: микродоғалық тотығу, титан, TiO_2 нанобөлшектері, коррозия, биоүйлесімділік, цитотоксикалық

А.Б. Кеңесбеков, А.Ж. Жасұлан, Н. Мұқтанова,
Дарын Байжан, Е. Ахметова, А. Серікбайқызы

Включение наночастиц TiO_2 для повышения коррозионной стойкости, цитосовместимости и антибактериальных свойств ПЭО-кальций-фосфатных покрытий на титане

Титан и его сплавы широко используются в биомедицинских имплантатах благодаря своим благоприятным механическим свойствам и коррозионной стойкости. Однако их нативная поверхность не обладает достаточной биоактивностью и антибактериальными свойствами. Микродуговое оксидирование является перспективным методом получения биоактивных покрытий, а включение наночастиц, таких как TiO_2, может дополнительно повысить их функциональность. Целью данного исследования было определение оптимальной концентрации наночастиц TiO_2 в электролите для микродугового оксидирования, обеспечивающей стабильность покрытия и биологическую безопасность. Покрытия из фосфата кальция были получены на технически чистом титане методом микродугового оксидирования с двумя концентрациями TiO_2: 0,5 мас.% (МАО 1) и 1 мас.% (МАО 2). Морфологию поверхности, пористость и фазовый состав анализировали методами сканирующей электронной микроскопии, энергодисперсионной спектроскопии и рентгеновской дифракции. Коррозионную стойкость оценивали методом потенциодинамической поляризации в растворах NaCl и Рингера, а биосовместимость — *in vitro* с использованием клеток остеосаркомы человека HOS и МТТ-теста. Увеличение содержания TiO_2 на 1 % уменьшало пористость покрытия (26,3 % против 13,7 % для МАО 1), улучшало защиту от коррозии и снижало коэффициент трения по сравнению с чистым титаном. Однако МАО 2 продемонстрировал высокую цитотоксичность (81 % гибели клеток) и частичную структурную деградацию в биологических средах. МАО 1 сохранял свою целостность и не оказывал токсического действия (3 % гибели клеток). Эти результаты свидетельствуют о том, что 0,5 % TiO_2 является оптимальной концентрацией для разработки безопасных покрытий для имплантатов, обеспечивая баланс между коррозионной стойкостью, механической стабильностью и биосовместимостью.

Ключевые слова: микродуговое оксидирование, титан, наночастицы TiO_2, коррозия, биосовместимость, цитотоксичность

Information about the authors

Kengesbekov, Aidar — PhD, D. Serikbayev East Kazakhstan Technical University, Ust-Kamenogorsk, Kazakhstan; e-mail: aidar.94.01@mail.ru; ORCID ID: https://orcid.org/0000-0002-5630-9467

Zhassulan, Ainur — PhD student, Engineering Center, Shakarim University NJSC, Semey, Kazakhstan; e-mail: a.zhassulan@shakarim.kz; ORCID ID: https://orcid.org/0009-0001-5887-0135

Muktanova, Nazerke — Researcher, D. Serikbayev East Kazakhstan Technical University, Ust-Kamenogorsk, Kazakhstan; e-mail: nmuktanova@bk.ru; ORCID ID: https://orcid.org/0000-0002-4823-6640

Daryn, Baizhan — PhD student, Shakarim University NJSC, Semey, Kazakhstan; e-mail: daryn.baizhan@mail.ru; ORCID ID: https://orcid.org/0000-0002-9105-3129

Ahmetova, Elvira — Researcher, D. Serikbayev East Kazakhstan Technical University, Ust-Kamenogorsk, Kazakhstan; e-mail: elya.akhmetova.04@mail.ru ORCID ID: https://orcid.org/0009-0000-4060-1001

Serikbaikyzy, Ainur (*corresponding author*) — PhD student, D. Serikbayev East Kazakhstan Technical University, Ust-Kamenogorsk, Kazakhstan; e-mail: ainura.serikbaikyzy@gmail.com; ORCID ID: https://orcid.org/0000-0003-4623-4681